ANALYSIS

17(47), 2020

ISSN
2319–7757
EISSN
2319–7765

Indian Journal of Engineering

Numerical simulation on the magnetic fluid flow through a channel

Saha S[1]✉, **Chakrabarti S**[2]

[1]Dept. of Mechanical Engineering, Academy of Technology, Aedconagar, Hooghly - 712121, West Bengal, India
[2]Department of Mechanical Engineering, Indian Institute of Engineering Science and Technology, Shibpur, Howrah -711103, West Bengal, India

✉**Corresponding author**
Dr. Sujoy Saha,
Associate Professor,
Department of Mechanical Engineering,
Academy of Technology, Aedconagar, Hooghly - 712121, West Bengal, India
Email†: sujoy.saha@aot.edu.in

Article History
Received: 3 November 2019
Accepted: 29 December 2019
Published: January 2020

Citation
Saha S, Chakrabarti S. Numerical simulation on the magnetic fluid flow through a channel. *Indian Journal of Engineering*, 2020, 17(47), 117-126

ABSTRACT

In order to solve the problem of high false positive rate of traditional SVD domain digital watermarking algorithm, a digital watermarking algorithm based on IWT and SVD is proposed. The algorithm firstly decomposes the carrier image into 1 IWT to obtain 4 subbands, then performs SVD transformation on the 4 subbands, and directly embeds the watermark image information into the singular values of the 4 subbands of the carrier image. In the process of embedding watermark, a digital signature authentication mechanism is proposed. The generated digital signature is used to encrypt the watermark image by embedding a

digital signature when the watermark is embedded. Before extracting the watermark, verify the digital signature to avoid false positives. Experiments show that the algorithm has good visibility and ability to resist various attacks.

Keywords: integer wavelet transform; singular value decomposition; digital signature; watermark; false alarm

1. INTRODUCTION

Dynamics of magnetic fluid in the emergence of magnetic field is having immense importance and implication in terms of use in industry, biotechnology and medical science areas. The flow of electrically conducting fluid in a channel in the presence of magnetic field has also become important because of its wide range of practical applications in diversified field, such as, combustor, mixing chamber, diffuser, heat exchanger, etc. The Magnetic Drug Targeting (MDT) and the Ferro fluid sealing are the example of medical applications. The magnetic fluids are also used in the MEMS field as a micro-fluid, driving and controller component. The course of magnetic fluid is tightly related to the external magnetic field and the condition of flow. Apart from that how its immovability and distributive behavior are influenced by the peripheral magnetic field along with the state of the flow, are very important. The mathematical modelling and the numerical simulations can significantly contribute to the further advancements of the above mentioned applications. For this purpose, a very first step is to obtain the fundamental insights of the underlying physics of flow (flow characteristics) of a magnetic fluid under the presence of the magnetic field. Magnetic fluids are a unique class of fluids. The dynamics of magnetic fluid in the existence of magnetic field is well recognized and capable of solving a large range of technical problems. There are many victorious applications of this magnetic fluid and also have massive future potential. In the present work, water base surfacted magnetic fluid has been used. The physical properties of the said fluid have been presented in the table 1 as of subsection 2.3.

The review of literature has been enriched with experimental, numerical and theoretical investigation of different researchers on magnetic fluid flow subjected to diverse magnetic field. From review of literature, it has been seen that, Hayat et al. [1] have investigated the influence of magnetic field on two-dimensional laminar and turbulent flow of fluid in a rectangular channel with taking into account both FHD and MHD phenomena. Takeuchi et al. [2] have experimental Study of MHD Effect on Turbulent Flow of Flibe Simulent Fluid in a Circular Pipe. Malekzadesh et al. [3] have experimentally investigated the influence of a magnetic field on steady, fully-developed laminar flow through a pipe. Khashan et al. [4] have studied a numerical simulation of magnetically mediated separation of labeled bio species from a native fluid flowing through a two dimensional channel. Hayat et al. [5] have analytically investigated the peristaltic MHD flow of a fluid in a channel under the influence of induced magnetic field with slip condition. Abd-Alla et al. [6] have studied the effect of magnetic field, rotation and initial stress on peristaltic motion of micropolar fluid in a flexible tube. Gedik et al. [7] have investigated a two-dimensional Computational Fluid Dynamics simulation for steady, laminar flow of an incompressible magneto rheological fluid between two fixed parallel plates in the presence of a uniform magnetic field. Galindo et al. [8] have studied both numerical and experimental modeling of a vertical gradient freeze type flow under the influence of both travelling and rotating magnetic fields. Srivastava and Deo [9] have studied the effect of transverse magnetic field on the viscous, incompressible, electrically conducting and fully developed flow of fluid through a porous medium of variable permeability.. Aminfar et al. [10] have studied the behaviour of ferrofluid in a tube with an elastic segment in the presence of non-uniform magnetic field. Akram et al. [11] have investigated the effect of induced magnetic field on the peristaltic transport of a fluid in a asymmetric channel. Bitla and Iyengar [12] have analytically investigated the pulsating flow of an incompressible and conducting micropolar fluid between two homogeneous permeable beds in the presence of an inclined uniform magnetic field. Muthtamilselvan and Doh [13] have executed a numerical investigation on laminar flow of nanofluid and mixed convective heat transfer in a cavity in the presence of a magnetic field. Azizian et al. [14] have experimentally investigated the effect of external magnetic field on laminar flow of magnetite nanofluids and convective heat transfer. Dritselis and Knaepen [15] have carried out their numerical simulation on convective heat transfer and fluid flow in a horizontal channel in the presence of uniform transverse magnetic field.

From the above mentioned review of literature, it is noted that a systematic detailed investigation considering the effect of Reynolds number on streamline contour, vorticity contour, wall shear stress distribution and wall static pressure distribution for two dimensional channel configuration is not addressed so far. Hence in this existing work, scrupulous effort has been given in order to study the flow characteristics of a magnetic fluid running through a channel with considering the principle of Magneto Hydro Dynamics (MHD).

2. MATHEMATICAL FORMULATION

A. Governing Equations

In this numerical investigation, viscous, electrically conducting, incompressible magnetic fluid subjected to axial magnetic field has been considered. The fig. 1 depicts the schematic diagram of the considered computational domain. The governing continuity and momentum equations are given by

$$\frac{\partial u}{\partial x}+\frac{\partial v}{\partial x} \tag{1}$$

$$\rho\left(u\frac{\partial u}{\partial x}+v\frac{\partial u}{\partial y}\right)=-\frac{\partial p}{\partial x}+\mu_0 M\frac{\partial H}{\partial x}-\sigma B^2 u+\mu\left(\frac{\partial^2 u}{\partial x^2}+\frac{\partial^2 u}{\partial y^2}\right)-\rho\frac{\partial(uv)}{\partial y} \tag{2}$$

$$\rho\left(u\frac{\partial v}{\partial x}+v\frac{\partial v}{\partial y}\right)=-\frac{\partial p}{\partial y}+\mu\left(\frac{\partial^2 v}{\partial x^2}+\frac{\partial^2 v}{\partial y^2}\right)-\rho\frac{\partial(uv)}{\partial x} \tag{3}$$

$$B=\mu_0 H \tag{4}$$

Where, μ_0 is the magnetic permeability of the magnetic medium, ρ is the fluid density, μ is the viscosity, H is the strength of considered magnetic field, σ is the electrical conductivity of water base magnetic fluid, B is the magnetic induction. These equations are also used by Hayat et al. [1] during their numerical work.

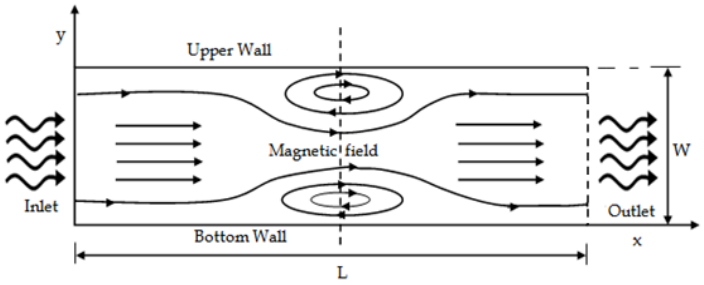

Figure 1 Schematic diagram of the computational domain and contours of the magnetic field strength H.

B. Boundary Conditions

The boundary conditions, which are being considered in the present problem, are as follows:

i) At the walls: at the walls fluid layers don't have any velocity, i.e., $u=0, v=0$

ii) At the inlet: at the inlet the horizontal component of velocity is specified and the vertical component of velocity is considered to be zero, i.e.,

$=\frac{R_e\,\mu}{\rho w}$, $v=0$

ii) At the outlet: at the outlet barometric pressure is specified.

The dimensionless parameters, which are been taken into account in this investigation, are

Magnetic number arising from MHD,

$$M=\frac{\mu_0^2 H^2 W^2 \sigma}{\mu}$$

Reynolds number,

$$R_e=\frac{\rho U W}{\mu}$$

C. Boundary Conditions

In this work water based magnetic fluid is used. In the Table 1 the properties of magnetic fluid, DI-water and magnetic nanoparticle (Fe_3O_4) are given.

Table 1 The highest magnitude of the upper wall and the bottom wall shear stress for different Reynolds number

Reynolds number	Highest magnitude of the upper wall shear stress and its position		Highest magnitude of the bottom wall shear stress and its position	
R_e	τ_u	L	τ_b	L
4200	8.424	0.699	10.547	0.686
4300	2.131	0.027	0.790	0.000
4500	7.611	0.028	0.853	0.000
4700	7.388	0.029	1.668	0.029
4800	2.289	0.011	0.906	0.000

D. Numerical Procedure

In this investigation, Finite volume method and SIMPLE algorithm have been used in order to solve continuity and momentum equations. The convection and diffusion terms of the governing equations are discretized by using power law scheme. The discretized equations have been solved repetitively with the help of line-by-line Alternating directional implicit (ADI) method. The length of the channel and height are considered to be 1.0 m and 0.05 m respectively for all calculations. The electrical conductivity (σ) for this work is assumed to be constant and equal to 1.0 x 10^6 /ohm- m. At the time the normalized residuals, which is summed over the whole calculation domain, fall below 10^{-6}, the convergence of the iterative scheme is considered to be achieved.

Now, after considering the pressure gradient term separately, the x-momentum discretization equation for the velocity of "u" becomes,

$$a_e\, u_e = \sum a_{nb}\, u_{nb} + b + (p_p - p_E)\, A_e$$

Similarly the other y-momentum discretization equation for velocity "v" can be written as

$$a_n\, v_n = \sum a_{nb}\, v_{nb} + b + (p_p - p_N)\, A_n$$

Here, the term $(p_p - p_E)A_e$ and other similar terms, represent the pressure force acting on respective control volume of the velocity, 'A' represents the area on which the pressure difference acts. The subscript 'nb' represents the neighbouring grid points.

At this point, we have come to know that if the pressure field is given or is somehow estimated, the momentum equation can be solved. It can also be said that unless the correct pressure field is used, the resulting velocity field does not satisfy the continuity equation. This type of velocity field, based on the guessed pressure field, denoted by p^*, is represented as, u^* and v^*. Therefore, the imperfect velocity field obtains from the solution of the following discretization equations:

$$a_e u_e^* = \sum a_{nb}\, u_{nb}^* + b + (p_p^* - p_E^*)\, A_e$$

$$a_n\, v_n^* = \sum a_{nb}\, v_{nb}^* + b + (p_p^* - p_N^*)\, A_n$$

Now our attempt should be to improve the guessed pressure p^* in such a way that the resulting imperfect velocity field progressively moves closer in satisfying the continuity equation. For that, let us propose the computation of correct pressure as, $p = p^* + p'$

Where, p' denotes the pressure correction. This change in the pressure certainly affects the velocity components. The

corresponding velocity corrections $u'$and v'can be similarly represented as, $u = u^* + u'$and $v = v^* + v'$.

If the equation

$$a_e u_e^* = \sum a_{nb}\, u_{nb}^* + b + \left(p_p^* - p_E^*\right) A_e$$

is subtracted from the equation, $a_e\, u_e = \sum a_{nb}\, u_{nb} + b + \left(p_p - p_E\right) A_e$

Then have $a_e u_e' = \sum a_{nb}\, u_{nb}' + \left(p_p' - p_E'\right) A_e$

Drop the term $\sum a_{nb}\, u_{nb}'$ then, the above equation will be as:

$$a_e u_e' = \left(p_p' - p_E'\right) A_e$$

Therefore the above equation can be written as, $u_e' = d_e\left(p_p' - p_E'\right)$,

Where $d_e = \frac{A_e}{a_e}$

So, velocity correction formula can be written as $u_e = u_e^* + d_e\left(p_p' - p_E'\right)$

This equation shows how the imperfect velocity u_e^* is to be corrected in response to the pressure correction to get u_e. The other velocity components can also be similarly written as, $v_n = v_n^* + d_n\left(p_p' - p_E'\right)$.

To get the pressure correction equation, velocity components are to be put into the discretized form of the continuity equation. Finally the discretization equation for pressure correction can be expressed as,

$$a_P p_P' = a_E p_E' + a_W p_W' + a_N p_N' + a_S p_S' + b_P$$

Where, a_E, a_W, a_N and a_s are the coefficients and b_P is the source terms for pressure node, and can be expressed by using the power low as,

$$a_E = \rho_e d_e \Delta y,$$

$$a_W = \rho_w d_w \Delta y,\ a_N = \rho_n d_n \Delta x,\ a_S = \rho_s d_s \Delta x$$

$$a_P = a_E + a_W + a_N + a_S$$

$$b_P = [(\rho u^*)_w - (\rho u^*)_e]\Delta y + [(\rho v^*)_s - (\rho v^*)_n]\Delta x$$

Now the discretization equation for velocity u can be expressed as

,

$$a_P u_P = \sum a_{nb}\, u_{nb} = a_E u_E + a_W u_W + a_N u_N + a_S u_S + b_u$$

Where, a_E, a_W, a_N, a_S and a_P are the coefficients and b_u is the source terms, and can be expressed by using the power low as,

$$a_E = D_e max[0, (1 - 0.1|P_e|)^5] + max(-F_e, 0)$$

$$a_W = D_w max[0, (1 - 0.1|P_w|)^5] + max(-F_w, 0)$$

$$a_N = D_n max[0, (1 - 0.1|P_n|)^5] + max(-F_n, 0)$$

$$a_S = D_s max[0, (1 - 0.1|P_s|)^5] + max(-F_s, 0)$$

$$a_P = a_E + a_W + a_N + a_S$$

$$b_u = (P_w - P_e)\Delta y + M_{nF}\Delta x \Delta y$$

where, D_e, D_w, D_n and D_s are the diffusion of flow per unit area at east, west, north and south face respectively , F_e, F_w, F_n and F_s are the mass flux per unit area of flow area at east, west, north and south face respectively , and P_e, P_w, P_n and P_s are the peclet number area at east, west, north and south face respectively, and can be expressed as,

$$D_e = \mu \frac{\Delta y}{\Delta x_e};\ F_e = (\rho u)_e \Delta y;\quad P_e = \frac{F_e}{D_e}$$

$$D_w = \mu \frac{\Delta y}{\Delta x_w};\ F_w = (\rho u)_w \Delta y;\ P_w = \frac{F_w}{D_w}$$

$$D_n = \mu \frac{\Delta x}{\Delta y_n};\ F_n = (\rho u)_n \Delta x;\quad P_n = \frac{F_n}{D_n}$$

$$D_s = \mu \frac{\Delta x}{\Delta y_s};\ F_s = (\rho u)_s \Delta x;\quad P_s = \frac{F_s}{D_s}$$

Similarly, the discretization equation for velocity v can be expressed as,

$$a_P v_P = \sum a_{nb}\, v_{nb} = a_E v_E + a_W v_W + a_N v_N + a_S v_S + b_v$$

3. RESULTS AND DISCUSSION

A. Variation of Streamline Contour and Vorticity Contour

From the maps of streamline contour of fig. 2, it has been observed that a number of recirculation zones have been formed closed to the walls of the channel. It has been also observed that with increasing the magnitude of Reynolds number the dimension of the recirculation region increases. The contour of vorticity depicts that, at the recirculation zones of channel the vorticities are formed and their concentration is increased with escalating Reynolds number. The reason may be the turbulence due to higher Reynolds number and the electromagnetic force due to MHD consideration. It has also been noted that the area and counting of recirculating region increased with increasing the magnitude of Reynolds number. Moreover, it is being anticipated that, the mixing rate in the mixing chamber and the diffusion in diffuser may be better with the increasing in vorticity and recirculating region. As a result of creation of bubbles and vorticity, the fluid retention time is likely to be greater. Consequently the heat transfer rate in micro heat exchangers may be expected to be more.

B. Variation of Wall Shear Stresses (WSS)

In this numerical study, the wall shear stress distribution has also been unerringly presented for different R_e with respect to its computed greatest magnitude. The greatest amplitude of WSS of 8.424 has been noted at the distance of 0.699 (i.e., L = 0.699) of the channel. That significant change in amplitude of upper WSS has been found in case of R_e = 4300. From fig, 3(a), it is noted that for all range of R_e of 3400, 4500, 4700, and 4800, the variation of top WSS is same, but, are dissimilar with respect to the maximum and the minimum amplitude and their location in the channel. The cause of creation of bubble, which has been correspondence in the earlier subsection, may be the reason behind the variation of upper WSS. The observation in this subsection has been substantiated by the earlier observation of streamline contour, which has been reported in the previous subsection 3.1. This magnitudes of upper WSS for different R_e ranging from 4200 to 4800 has also been presented in tabular form (i.e., table 1), considering the same condition used in fig. 3(a).

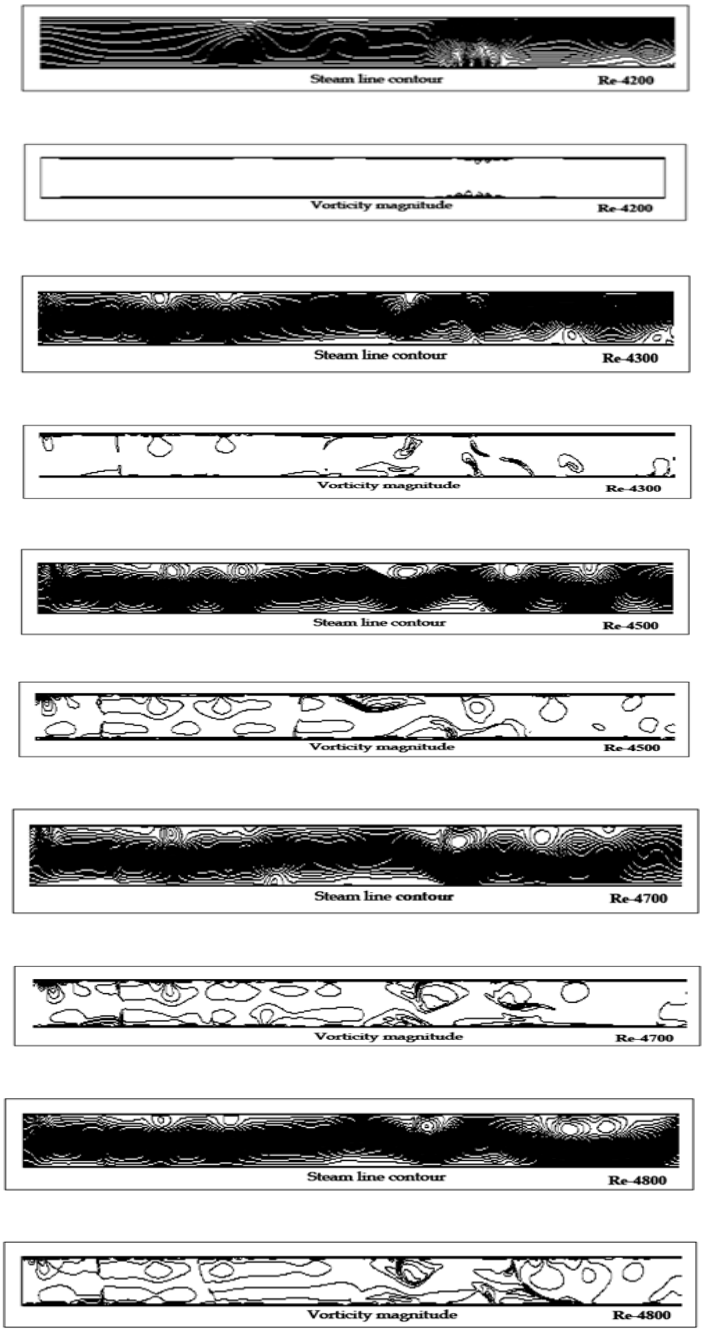

Figure 2 Stream line and vorticity contour for Magnetic number of 3.66 and for different Reynolds numbers

Fig. 3(b) depicts, the lower WSS distribution with taking into account the same range of R_e. For all the considered R_e similar kind of variation lower WSS has been noted, but remarkable fluctuation has been seen case of R_e = 4300. The mentioned table 1 shows, the height values of bottom WSS and their corresponding location in the channel, considering the same condition as used in fig. 3(b). From the table, it has been noted that with reducing Reynolds number, both the WSS increases. The Reynolds number is inversely proportional to viscous force, hence, with the decrease in Reynolds number shear stress increases. This may be the probable explanation behind the present findings. Therefore, it may also be ascertained that existing physics authenticates the present observations.

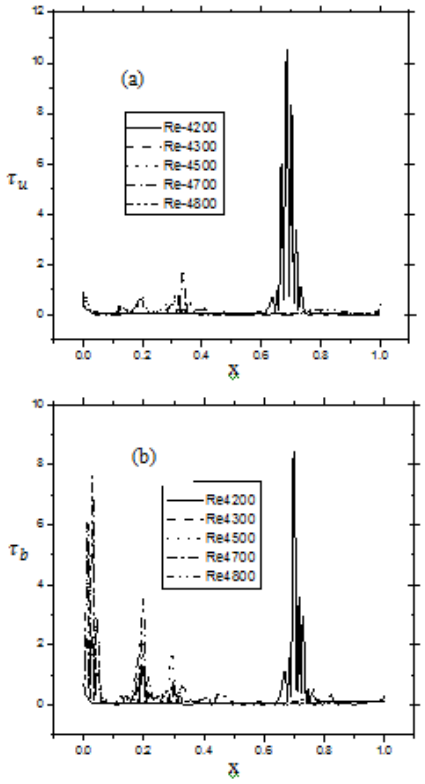

Figure 3 Variation of the Upper and the bottom wall shear stress for the different Reynolds number

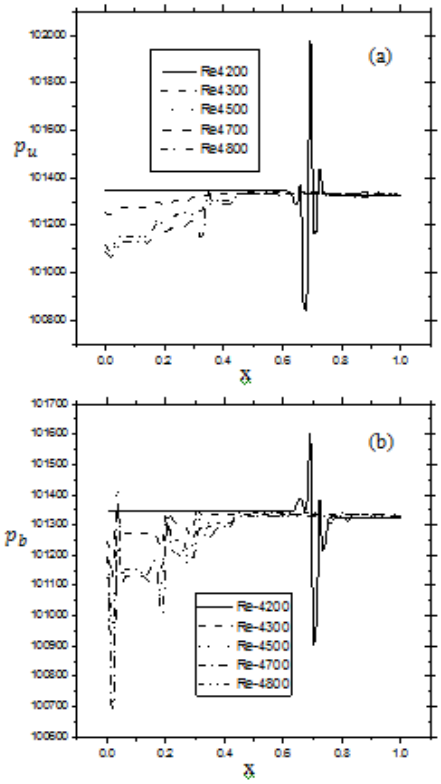

Figure 4 Upper and bottom wall static pressure at different position for different Reynolds number

C. Variation of Wall Static Pressure

Fig. 4(a) depicts the distribution of wall static pressure over the entire length of the channel with respect to different R_e. It has been

noted that the amplitude of pressure frequently changes from inlet to exit. The probable reason may be attributed due to the electromagnetic force, which is acting on the magnetic particles of fluid. The formation of vorticity zone and recirculating bubbles in the test section may be another reason behind the observation. Moreover, it is seen that, even though similar type of variations of pressure have been taken place in test section for all considered Reynolds numbers (R_e) of 4200, 4300, 4500, 4700, and 4800, but those are dissimilar in terms of their amplitude and location. The maximum and minimum amplitudes of pressure along with its location have been introduced in table 2.

Table 2 The highest and lowest magnitude of upper wall pressure for different Reynolds number

R_e	**Highest magnitude and its position**		**Lowest magnitude and its position**	
R_e	p_{stu}	L_h	p_{stu}	L_l
4200	101601	0.691	100503	0.704
4300	101358	0.036	101125	0.017
4500	101423	0.036	100715	0.018
4700	101357	0.037	100695	0.019
4800	101343	0.624	100979	0.019

Table 3 The highest and lowest magnitude of bottom wall pressure for different Reynolds number

R_e	**Highest magnitude and its position**		**Lowest magnitude and its position**	
R_e	p_{stu}	L_h	p_{stu}	L_l
4200	101977	0.694	100842	0.680
4300	101337	0.848	101243	0.071
4500	101334	0.463	101094	0.019
4700	101341	0.347	101069	0.015
4800	101342	0.620	101094	0.015

Fig. 4(b) depicts the lower wall static pressure distribution in the test section. The causes of such variation have been mentioned earlier. The maximum and minimum amplitude of pressure and its corresponding position have been submitted in the table 3 considering the same conditions, which is used in fig. 4(b). From tables it can be mentioned that, with increasing R_e pressure decreases in the test section. In this regards, it may be mentioned that the magnetic force, which is acting on the fluid particles, reduces with decrease in R_e.

Thus, due to the less amount of retarding force, the velocity of flow as well as kinetic energy increases. Therefore, the pressure energy at lower Reynolds number increases. This may be the probable reason behind this observation. Lower Reynolds number may be used to improve the performance of industrial equipments such as turbine, compressor, etc.

4. CONCLUSION

From the exercise, the following conclusions have been made:

1. For Reynolds number of 4800, the number of recirculating bubbles is highest.
2. Both the upper and bottom wall shear stresses obtain their highest magnitude of 8.424 and 10.547 respectively at Reynolds number of 4200.
3. For Reynolds number of 4200, the magnitude of upper wall static pressure and bottom wall static pressure becomes highest and is equal to 101609 and 101977 respectively.

Acknowledgement

I would like to acknowledge the Prof. Dlip Bhattacharya, Director of Academy of Technology, Prof. Jagannath Banerjee, Founder & Chairman Trustee of Academy of Technology, Head, faculties and staff members of Mechanical Engineering Department for their continuous encouragement.

Contribution of authors

Entire work has been done by Dr. S. Saha including writing of the paper and the same has been supervised by Dr. S. Chakrabarti

Funding: This research received no external funding.

Potential conflict of interests

1. The fundamental problem of two dimensional, viscous, electrically conducting water base magnetic fluid, flowing through a channel subjected to magnetic field with considering Magneto Hydro Dynamics (MHD) phenomenon is numerically studied.
2. During the simulation the Magnetic number arising from Magneto Hydro Dynamics (MHD) of 3.66 and Reynolds numbers ranging from 4200 to 4800 have been used
3. The effect of Reynolds number on streamline contour, vorticity contour, wall shear stress and wall static pressure has been presented in the results and discussion section in detail.

REFERENCE

1. T. Hayat, A. Afsar, M. Khan M, S. Asghar. Peristaltic transport of a third order fluid under the effect of a magnetic field. *Comput. Math. Appl*. 2007; 53: 1074-87.
2. J. Takeuchi, SI. Satake, NB. Morley, T. Kunugi, T. Yokomine, MA. Abdou. Experimental study of MHD effects on turbulent flow of Flibe Simulent fluid in circular pipe. *Fusion. Eng. Des.* 2008; 83: 1082-6.
3. Malekzadeh, A. Heydarinasab, M. Jahangiri. Magnetic field effect on laminar heat transfer in a pipe for thermal entry region. *J. Mech. Sci. Technol.* 2011; 25: 877-84.
4. SA. Khashan, E. Elnajjar, Y. Haik. Numerical simulation of the continuous biomagnetic separation in a two-dimensional channel. *Int. J. Multiphas Flow*. 2011; 37: 947-55.
5. T. Hayat, S. Noreen, A. Alsaedi. Slip and induced magnetic field effects on peristaltic transport of Johnson-Segalman fluid. *Appl. Math. Mech.* 2012; 33: 1035-48.
6. AM. Abd-Alla, GA. Yahya, SR. Mahmoud, HS. Alosaimi. Effect of the rotation, magnetic field and initial stress on peristaltic motion of micropolar fluid. *J. Meccanica.* 2012; 47: 1455-65.
7. E. Gedik, H. Kurt, Z. Recebli, C. Balan. Two-dimensional CFD simulation of magnetorheological fluid between two fixed parallel plates applied external magnetic field. *Comput. Fluids.* 2012; 63: 128-34.
8. V. Galindo, K. Niemietz, O. Pätzold, G. Gerbeth. Numerical and experimental modeling of VGF-type buoyant flow under the influence of traveling and rotating magnetic fields. *J. Cryst. Growth*. 2012; 360: 30-4.
9. BG. Srivastava, S. Deo. Effect of magnetic field on the viscous fluid flow in a channel filled with porous medium of variable permeability. *Appl. Math. Comput*. 2013; 219: 8959-64.
10. H. Aminfar, M. Mohammadpourfard, F. Ghaderi. Two-phase simulation of non-uniform magnetic field effects on biofluid (blood) with magnetic nanoparticles through a collapsible tube. *J. Magn. Magn. Mater*. 2013; 332: 172-9.
11. S. Akram, S. Nadeem, M. Hanif. Numerical and analytical treatment on peristaltic flow of Williamson fluid in the occurrence of induced magnetic field. *J. Magn. Magn. Mater*. 2013; 346: 142-51.
12. P. Bitla, TKV. Iyengar. Pulsating flow of an incompressible micropolar fluid between permeable beds with an inclined uniform magnetic field. *Eur. J. Mech. B. Fluids*. 2014; 1-16.
13. M. Muthtamilselvan, DH. Doh. Magnetic field effect on mixed convection in a lid-driven square cavity filled with nanofluids. *J. Mech. Sci. Technol.* 2014; 28: 137-43.
14. R. Azizian, E. Doroodchi, T. McKrell, J. Buongiorno, LW. Hu, Moghtaderi B. Effect of magnetic field on laminar convective heat transfer of magnetite nanofluids. *Int. J. Heat Mass Transfer*. 2014; 68: 94-109.
15. CD. Dritselis, B. Knaepen. Mixed convection of a low Prandtl fluid with spatially periodic lower wall heating in the presence of a wall-normal magnetic field. *Int. J. Heat Mass Transfer*. 2014; 74: 35-47.